Hindawi
Advances in Multimedia
Volume 2023, Article ID 9841914, 1 page
https://doi.org/10.1155/2023/9841914

Retraction

Retracted: Effect of Gradient Doping on Charge Collection Efficiency of EBCMOS Devices

Advances in Multimedia

Received 12 December 2023; Accepted 12 December 2023; Published 13 December 2023

Copyright © 2023 Advances in Multimedia. This is an open access article distributed under the Creative Commons Attribution License, which permits unrestricted use, distribution, and reproduction in any medium, provided the original work is properly cited.

This article has been retracted by Hindawi, as publisher, following an investigation undertaken by the publisher [1]. This investigation has uncovered evidence of systematic manipulation of the publication and peer-review process. We cannot, therefore, vouch for the reliability or integrity of this article.

Please note that this notice is intended solely to alert readers that the peer-review process of this article has been compromised.

Wiley and Hindawi regret that the usual quality checks did not identify these issues before publication and have since put additional measures in place to safeguard research integrity.

We wish to credit our Research Integrity and Research Publishing teams and anonymous and named external researchers and research integrity experts for contributing to this investigation.

The corresponding author, as the representative of all authors, has been given the opportunity to register their agreement or disagreement to this retraction. We have kept a record of any response received.

References

[1] X. Qin, Q. Shi, F. Shi, Y. Li, and D. Song, "Effect of Gradient Doping on Charge Collection Efficiency of EBCMOS Devices," *Advances in Multimedia*, vol. 2022, Article ID 5157252, 8 pages, 2022.

Hindawi
Advances in Multimedia
Volume 2022, Article ID 5157252, 8 pages
https://doi.org/10.1155/2022/5157252

RETRACTED

Research Article

Effect of Gradient Doping on Charge Collection Efficiency of EBCMOS Devices

Xulei Qin ,[1,2] Qidong Shi ,[2] Feng Shi ,[1] Ye Li ,[2] and De Song [2]

[1] *National Key Laboratory of Science and Technology on Low-Level-Light, Xi'an 710065, China*
[2] *Changchun University of Science and Technology, Changchun 130022, China*

Correspondence should be addressed to Xulei Qin; qxl@cust.edu.cn

Received 13 July 2022; Revised 6 August 2022; Accepted 9 August 2022; Published 29 August 2022

Academic Editor: Tao Zhou

Copyright © 2022 Xulei Qin et al. This is an open access article distributed under the Creative Commons Attribution License, which permits unrestricted use, distribution, and reproduction in any medium, provided the original work is properly cited.

We investigated the effect of different gradient doping methods on the charge collection efficiency of the electron multiplication layer of EBCMOS devices. Exponential doping of the electron multiplication layer can form a built-in electric field in the electron multiplication layer that is favorable for photoelectron transport, so exponential doping instead of uniform doping in the electron multiplication layer of EBCMOS can effectively improve the charge collection efficiency. It is shown that exponential heavy doping on the side of the electron multiplication layer near the dead layer and exponential light doping on the side near the depletion region can improve the built-in electric field structure and increase the lifetime of the multiplied electrons, thereby improving the charge collection efficiency of EBCMOS. The optimized device achieves a charge collection efficiency of 94.48% at an incident electron energy of 4 keV, an electron beam diameter of 20 nm, a dead layer thickness of 60 nm, and a *P*-type silicon epitaxial layer thickness of 10 μm.

1. Introduction

Current micro-optical imaging devices are mainly divided into ICCD, EMCCD, EBCMOS, and so on [1]. EBCMOS uses a thinned P-type silicon substrate as the electron multiplication layer to replace the traditional ICCD microchannel plate, fluorescent screen, and coupling device [2], thus making the device size significantly reduced [3]. The electrons generate a large number of electron-hole pairs within the electron multiplication layer, and the obtained electron bombardment semiconductor gain noise is low [4, 5], making the imaging performance of EBCMOS devices far superior to EMCCD devices [6, 7]. With the advantages of small size, low power consumption, fast response, and high resolution [8], EBCMOS devices are widely used in security, biological [9, 10], and medical fields [11, 12].

In 1999, after Intevac published the patent for the EBCMOS device, the first EBCCD with GaAs as the photocathode was subsequently released [13]. After that, because CMOS devices are superior compared to CCD devices, CMOS devices gradually replaced CCD devices [14], and in 2000, Aebi and Boyle [15] developed the world's first EBCMOS devices [15]. After that, depending on the continuous maturity of CMOS technology, EBCMOS devices began to gradually move towards the trend of high resolution and high frame rate. In 2005 Intevac launched ISIE6 and ISIE10 can reach a high resolution of 1280 $*$ 1024, compared to the previous generation of EBCMOS devices significantly reducing the read noise [16], while the reduced pixel size has also greatly improved the imaging sensitivity of the device [17]. In 2007, the University of Lyon in France, in cooperation with the University of Strasbourg and Photonis, released an EBCMOS device called EBMIMOSA5, which enabled single-photon detection. In 2008, the University of Lyon produced the LUSIPHER [18], a sensor with an increased imaging frame rate from 40 FPS in the EBMIMOSA5 to 500 FPS, which substantially improved single-molecule tracking and allowed the device to be applied in single-molecule tracking experiments. In 2010, Photonis released the EBNoctun1.3Mpx and EBNoctun2Mpx cameras with resolutions of 1.3 and 2 megapixels, respectively. Both can work normally under 10^{-5}lx and can reach 60fps. In 2011,

R. Barbier et al. of the University of Lyon used LUSIPHER to achieve single-photon imaging [19]. In 2012, due to its high sensitivity, the University of Lyon used an improved EBCMOS camera system called LuSEApher to achieve deep-sea marine bioluminescence recordings at high frame rates and high sensitivity states [20].

In EBCMOS devices, the incident photoelectrons are accelerated by the accelerating electric field and then enter the BSB-CMOS anode [21], consume a certain amount of energy to cross the dead layer, and then enter the thinned *P*-type silicon substrate [22], where the photoelectrons collide and scatter with the atoms in the electron multiplication layer, which can be classified into elastic scattering and inelastic scattering according to whether energy is consumed [23]. The elastic scattering process changes the direction of electron motion but does not lose energy while the inelastic scattering process not only changes the direction of electron motion but also loses energy [24]. During inelastic scattering, electrons collide with atoms in the electron multiplication layer, generating a large number of electron-hole pairs. The multiplied electrons are transported to the N-well for collection by diffusion and drift under the action of the electric field and concentration gradient built into the electron multiplication layer and are finally read by the image element circuit [25]. The different doping of the electron multiplication layer determines the distribution of the built-in electric field in the EBCMOS electron multiplication layer. A suitable electric field distribution can increase the electron transport speed and improve the charge collection efficiency. So, the doping of the electron multiplication layer can be changed to improve the charge collection efficiency of the EBCMOS device and thus enhance the imaging level.

In this paper, the effect of different doping methods on the electric field distribution is investigated, and the effect of doping concentration on the minority carriers' lifetime is also combined with the Monte-Carlo method to obtain the charge collection efficiency under different gradient doping methods, so as to provide a theoretical basis for obtaining EBCMOS devices with high imaging quality.

2. Simulation of the Distribution of Multiplying Electrons in the Electron Multiplication Layer

2.1. Electron Multiplication Process in the Electron Multiplication Layer. The EBCMOS device uses a photocathode as the cathode of the device and a thin-backed CMOS sensor as the anode of the device [26]. The photocathode and the BSB-CMOS are encapsulated in a vacuum tube [27], the structure of which is shown in Figure 1.

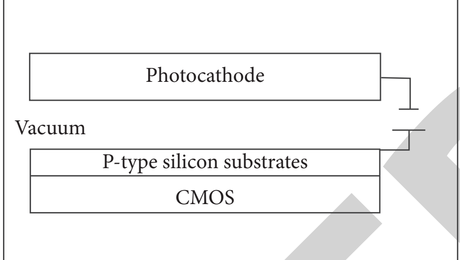

Figure 1: Structure of EBCMOS image sensor.

After the external photons are incident on the photocathode, the photocathode releases photoelectrons, which gain energy to accelerate under the acceleration of the near-focus structure and bombard the BSB-CMOS [28]. After the photoelectrons consume certain energy to cross the dead layer, collisions occur between the electron multiplication layer region and the solid atoms, and then a large number of electron-hole pairs are generated [29], and a part of the holes generated in this process will gradually move toward the dead layer and disappear, and a part of the holes will compound with the electrons and disappear. The concentration gradient causes the generated multiplier electrons to diffuse toward the depletion region, while the built-in electric field in the electron multiplication layer causes the multiplier electrons to drift toward the depletion region [30]. Eventually, the multiplier electrons are collected at the N-well, and a high multiplicative gain is obtained [31, 32]. Since the ionization energy of *P*-type silicon is 3.6 Ev [33], the obtained electron bombardment semiconductor gain can be expressed by the following equation [34], where E_0 is the energy of photoelectrons incident on the anode, E_{Dead} is the energy consumed by photoelectrons crossing the dead layer, ε is the charge collection efficiency, and G is the obtained electron bombardment semiconductor gain multiplier.

$$G = \frac{\varepsilon\left(E_0 - E_{\text{Dead}}\right)}{3.65}. \quad (1)$$

Doping the *P*-type silicon substrate can generate a corresponding built-in electric field in the electron multiplication layer. Under the effect of the built-in electric field, the multiplication of electrons will accelerate to drift toward the depletion region and be collected by the N-well, thus enhancing the charge collection efficiency.

2.2. Elastic Scattering Model of Incident Electrons in the Electron Multiplication Layer. In the elastic scattering process [35], photoelectrons pass through the dead layer and collide with the nucleus. The energy loss of the incident electrons during the whole process is so small that it can even be negligible. We analyze the collisions for a single atom using the classical Rutherford formula, which can then be extended to the elastic scattering process for all atoms.

In the process of applying the classical Rutherford formula, we need to neglect the volume of the electron itself and assume that the electron is attracted by the nucleus. At the same time, the electron is shielded by the Coulomb force when the formula for the differential scattering cross-section of the electron satisfies the following equation:

$$\frac{d\sigma_i(\theta)}{d\Omega} = \frac{e^4 Z_i\left(Z_i + 1\right)}{64\pi^2\varepsilon_0^2 E^2}\left(\frac{E + m_e C^2}{E + 2m_e C^2}\right)\frac{1}{\left(\sin^2(\theta/2) + \beta_i\right)^2}, \quad (2)$$

where e is the electric charge of a single atom, m_e is the mass of an electron, E is the energy of an electron, ε_0 is the dielectric constant, Z_i is the atomic number of an atom in a solid, and β_i is the shielding factor.

RETRACTED

In order to avoid breakdown, the voltage between the photoelectric cathode and photoelectric anode is generally less than 8 kV, which means that the incident photoelectron energy is generally lower than 10 keV. At this time, the use of the classical Rutherford formula will produce a large error. For this reason, we use the Rutherford formula for further correction. After the correction of the Rutherford formula for the incident light electron energy for the range of 0.1 ~ 30 keV [36], the formula is as follows:

$$\sigma_T = \frac{3.0 \times 10^{-18} Z^{1.7}}{\left(\left(E + 0.005 Z^{1.7} E^{0.5} + 0.0007 Z^2\right)/\left(E^{0.5}\right)\right)} \mathrm{cm}^2. \tag{3}$$

2.3. Inelastic Scattering Model of Incident Electrons in the Electron Multiplication Layer. In the inelastic scattering process, electrons gain electron gain after the excitation of secondary electrons while the process of excitation of electrons in the process of multiple collisions gradually loses energy, and the single energy loss is much smaller than the initial energy of the incident electrons, so the single energy loss can be calculated using the Bethe energy loss formula. Each inelastic scattering collision is considered an independent event [37, 38], and its energy loss formula is expressed as follows:

$$-\frac{dE(\theta)}{dS} = \frac{2\pi e^4}{E_0} nZ \ln \frac{1.166E}{J}. \tag{4}$$

Due to the low energy of the incident electrons, we found that the final calculated energy loss was not true during the actual use of the Bethe energy loss formula. For this reason, we instead used the modified Bethe formula proposed by Joy and Lou for low-energy electrons.

$$\frac{\mathrm{d}E(\theta)}{\mathrm{d}S} = -7.85 \times 10^4 \frac{\rho Z}{AE_0} \ln \frac{1.166\left(E_0 + kJ\right)}{J}. \tag{5}$$

In the above-given equation, A is the atomic weight, Z is the atomic number, E_0 is the energy contained in the electron, ρ is the density of the medium, and k is the correction factor. In this paper, since the substrate material is silicon, its atomic number is low, and according to the relationship between k and the atomic number when the atomic number of the medium is low, there is the equation

$$\frac{k_{Al} - k_C}{k_C - k_{Si}} = \frac{Z_{Al} - Z_C}{Z_C - Z_{Si}}. \tag{6}$$

It is known that $K_{Al} = 0.815$ and $K_c = 0.77$, and bringing in the known values gives $K_{Si} = 0.822$.

2.4. The Trajectory of Electrons in the Electron Multiplication Layer. In general, since the doping concentration of P-type impurities in the electron multiplication layer is not higher than 10^{19} atoms/cm^3, the doped boron atom concentration to silicon atom concentration ratio is lower than 1 : 100 [39], and the effect of electron collision with boron atoms can be disregarded in the electron multiplication process. During the motion of electrons in the multiplication layer, the trajectory is mainly determined by the following four variables, namely, electron energy E, electron scattering angle θ, scattering azimuth angle φ,, and scattering step Λ [40]. Among them, the electron scattering angle θ satisfies the following equation:

$$\cos\theta = 1 - \frac{2\beta_i R}{1 + \beta_i - R}, \tag{7}$$

where $\beta_i = 3.4 \times 10^3 (Z_i^{(2/3)}/E)$ which is the Rutherford elastic scattering shielding coefficient and R is a random number within (0, 1).

The scattering azimuth angle φ satisfies the following equation:

$$\varphi = 2\pi R. \tag{8}$$

Scattered step length Λ satisfies the following equation:

$$\Lambda = -\frac{A}{N_A \rho \sigma_T} \ln R, \tag{9}$$

where N_A is Avogadro's constant and σ_T is the total elastic scattering cross-section.

In the process of elastic scattering calculation, it is only necessary to consider the relative change of coordinates at the end of each process compared to the coordinates after the previous scattering, calculate this cumulatively in the z-direction, and stop the calculation when the distance in the z-direction is greater than the thickness of the electron multiplication layer [41].

In the inelastic scattering process, not only the orientation of the electron scattering motion should be calculated but also the energy lost in the single inelastic scattering process should be calculated at the same time. After each inelastic scattering process calculation, the remaining energy of the obtained electron will be used as the initial energy for the next calculation, and the position of the obtained electron will be used as the initial position for the next calculation, and if the electron energy is less than 3.6 eV, the calculation will be stopped at this time.

The energy remaining in the electron after the nth scattering can be expressed by the following equation:

$$E_{n+1} = E_n - \frac{dE}{ds}\Big|_{E_n} \cdot \Lambda_n. \tag{10}$$

The change in spatial position of the scattered electron after a single scattering process can be expressed by the following equation:

$$\begin{cases} x_n = x_{n-1} + r\sin\theta\cos\phi, \\ y_n = y_{n-1} + r\sin\theta\sin\phi, \\ z_n = z_{n-1} + r\cos\theta. \end{cases} \tag{11}$$

3. Electric Field Distribution inside the Electron Multiplication Layer with Different Doped Methods

3.1. Distribution of Electric Field in Electron Multiplication Layer with Uniformly Doped Methods. The electron multiplication layer is uniformly doped, and such doping leads to

RETRACTED

the generation of an internal electric field in the depletion region, and the electric field distribution is shown in Figure 2. After the photoelectrons pass through the dead layer into the electron multiplication layer, collisional scattering with atoms occurs, and multiplication electrons are generated during inelastic collisions. The multiplication process of electrons is regarded as the injection of nonequilibrium carriers. At this time, the multiplier electrons diffuse towards the depletion region under the influence of the concentration gradient, and the following equation gives the diffusion velocity of carriers:

$$v_{d(r)} = -\left[\frac{D_n}{r} + \frac{D_n}{L_n}\right]. \tag{12}$$

At this time, the trajectory of the multiplier electrons can be expressed by the following equation:

$$\begin{cases} t_{(i)} = \dfrac{L_i}{v_z}, \\ x_i = v_{(x)} \cdot t + x_{(i-1)}, \\ y_i = v_{(y)} \cdot t + y_{(i-1)}. \end{cases} \tag{13}$$

In the depletion region, the effect of the built-in electric field makes the electron migration velocity much faster than the electron diffusion velocity, and the electron migration is accelerated toward the N-well.

3.2. Distribution of Electric Field during Exponential Doping of Electron Multiplication Layer. We found that when the p-type silicon substrate is uniformly doped, there is only an electric field distribution in the depletion region, and the multiplication of electrons in the electron multiplication layer only depends on the concentration gradient for diffusion. At this time, increasing the transport velocity of multiplier electrons can reduce the recombination rate of electron-hole pairs, thus increasing the charge collection efficiency. In order to enhance the transport velocity of multiplier electrons, a gradient electric field can be generated at the P-type silicon substrate by exponential doping of the P-type silicon substrate, and the electric field distribution at this time is shown in Figure 3. Different gradient index doping methods have a significant effect on the distribution of the electric field outside the depletion region [42], so changing the gradient index doping method can effectively improve the charge collection efficiency.

The doping concentration profile of the P-type silicon substrate satisfies the following equation:

$$N_Z = N_0 \exp(-b_i \cdot z), \tag{14}$$

where N_z is the doping concentration at different locations of the P-type silicon substrate along the z-axis direction, z is the coordinate of the specific location, N_0 is the doping concentration at $z=0$, and b_i is a calculated parameter

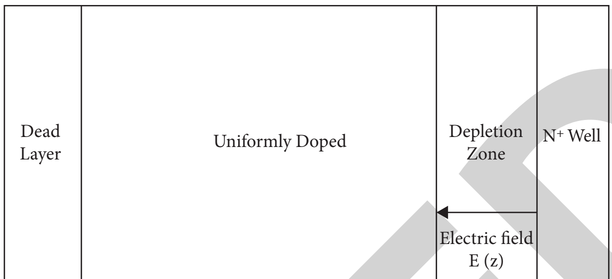

Figure 2: Electric field distribution model for uniform doping of electron multiplication layer.

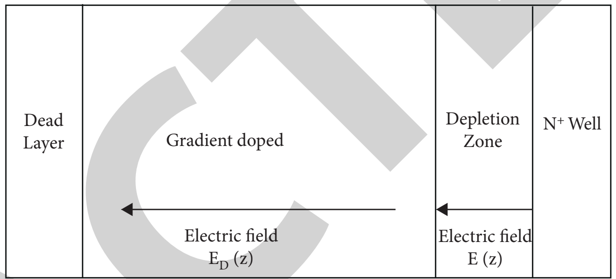

Figure 3: Electric field distribution model for exponential doping of electron multiplication layer.

determined by the beginning and end doping concentrations and the beginning and end distances.

The electric field intensity in the exponentially doped region is the following equation:

$$E_D(z) = \frac{kT}{q} \cdot b_i, \tag{15}$$

where the Boltzmann constant $k = 1.38 \times 10^{-23}$ J/K, $T = 300$ K at room temperature, and $q = 1.6 \times 10^{-19°}$C. At this point, the diffusion velocity of carriers satisfies the following equation:

$$v_{d(r)} = -\left[\frac{D_n}{r} + \frac{D_n}{2L_n^2} \cdot \left(\sqrt{L_n^2(E) + 4L_n^2} - L_n(E)\right)\right]. \tag{16}$$

The drift velocity of the carrier is given by the following equation:

$$\begin{cases} v_{(x)} = v_{d(r)} \cdot \sin\theta_i \cdot \cos\phi, \\ v_{(y)} = v_{d(r)} \cdot \sin\theta_i \cdot \sin\phi, \\ v_{(z)} = v_{d(r)} \cdot \cos\theta_i + v_{E(z)}. \end{cases} \tag{17}$$

D n is the diffusion coefficient, the carrier diffusion length $L_n = \sqrt{D_n \cdot \tau_n}$, τ is the lifetime of the nonequilibrium carrier, $L_n(E) = (\mu_n E\tau/cos\theta_i)$, $v_{E(z)} = \mu_n \cdot E$, μ_n is the electron mobility, and the electron mobility is related to the doping concentration.

When the electron multiplication layer is exponentially doped, the motion trajectory of the multiplication electrons is shown in Figure 4. When $v_{(z)} < 0$, the multiplier electrons move toward the dead layer and are finally compounded; when $v_{(z)} > 0$, the multiplier electrons move toward the N-well and are finally collected.

RETRACTED

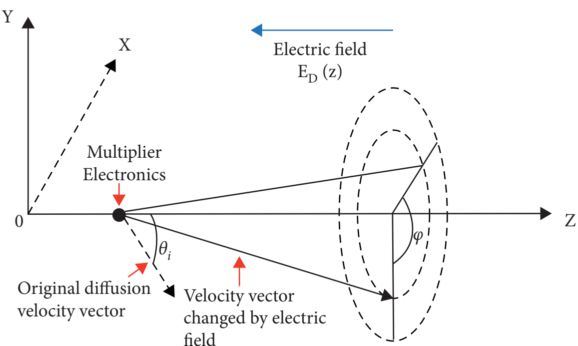

FIGURE 4: Changes in the trajectory of electron motion under the action of gradient electric field.

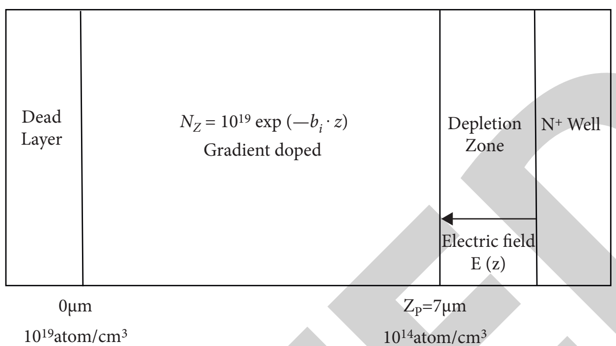

FIGURE 5: *P*-type silicon epitaxial layer overall index doping model.

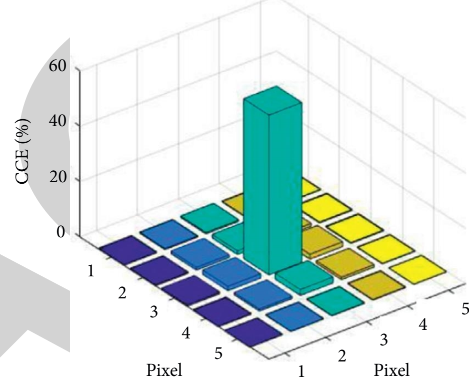

FIGURE 6: Charge collection efficiency in the 5×5 pixel region.

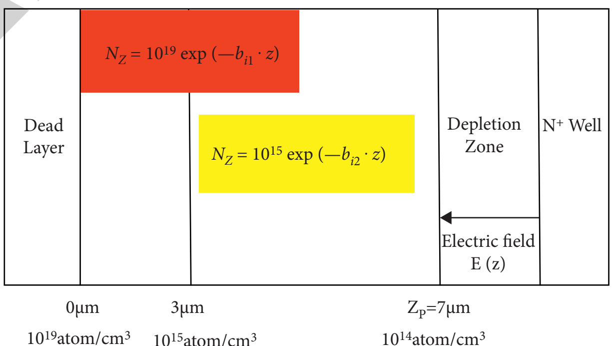

FIGURE 7: Electron multiplication layer multisegment exponential doping structure model1.

4. Charge Collection Efficiency under Different Gradient Doping Methods and Discussion

According to the semiconductor theory, by combining the parameters such as lifetime, depletion region width, and diffusion coefficient of nonequilibrium carriers under different gradient doping methods, the trajectories of corresponding multiplier electrons in the substrate can be obtained, and finally, the charge collection efficiency under different gradient doping can be obtained. In the simulation parameters, the incident electron energy is set to 4 keV, the electron beam diameter is 20 nm, the dead layer thickness is 60 nm, and the thickness of the P-type silicon epitaxial layer is 10 μm.

At $0 < z < 7$, the overall exponential doping is performed with $N_Z = 10^{19}\exp(-b_i \cdot z)$ and $N_7 = 10^{14}$atom/cm^3. Figure 5 shows the electron multiplication layer model for this doping method.

At this time, the electron distribution in the 5×5 region is shown in Figure 6, and the final obtained charge collection efficiency is 54.74%.

In this doping method, although a gradient electric field is generated in the *P*-type silicon epitaxial layer and the multiplier electrons change their trajectories under the influence of the gradient electric field, the obtained charge collection efficiency is only 54%. The charge collection efficiency at this point is mainly limited by the non-equilibrium carrier lifetime and the strength of the built-in electric field in this doping mode. In P-doped silicon, the lifetime of the non-equilibrium carriers is given by the following equation:

$$\tau_n = \left(3.45 \times 10^{-12} N_A + 9.5 \times 10^{-32} N_A^2\right)^{-1}, \quad (18)$$

where N_A is the concentration of impurities. We can improve the gradient electric field distribution of the *P*-type silicon epitaxial layer by changing the doping structure to improve the lifetime of the nonequilibrium carriers and finally obtain a higher charge collection efficiency.

At $0 < z < 3$, exponential doping is performed with $N_Z = 10^{19}\exp(-b_{i1} \cdot z)$, and at $3 < z < 7$, exponential doping is performed with $N_Z = 10^{15}\exp(-b_{i2} \cdot z)$, $N_3 = (10^{15}$atom/cm$^3)$. Figure 7 shows the electron multiplication layer model for this doping method.

The electron distribution in the 5×5 region at this time is shown in Figure 8, and the final charge collection efficiency obtained is 70.35%.

With this doping, the charge collection efficiency reaches 70.35%. In order to enhance the nonequilibrium carrier lifetime, we will try to further thin the thickness of the exponential heavily doped layer to achieve the effect of increasing the charge collection efficiency.

At $0 < z < 0.5$, exponential doping is performed with $N_Z = 10^{19}\exp(-b_{i3} \cdot z)$, and at $0.5 < z < 7$, exponential doping is performed with $N_Z = 10^{15}\exp(-b_{i4} \cdot z)$, $N_{0.5} = (10^{15}$atom/cm$^3)$, and Figure 9 shows the model of electron multiplication layer for this doping method.

RETRACTED

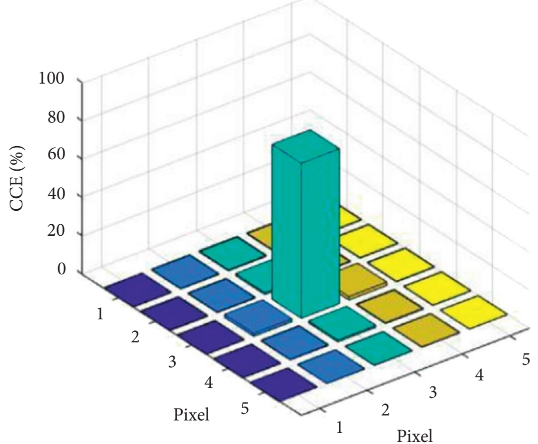

Figure 8: Charge collection efficiency in the 5 × 5 pixel region.

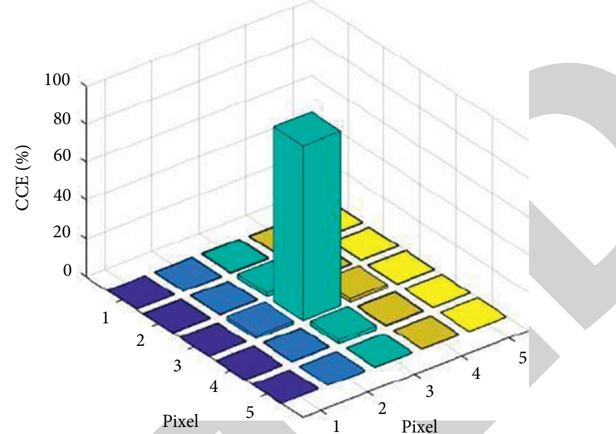

Figure 10: Charge collection efficiency in the 5 × 5 pixel region.

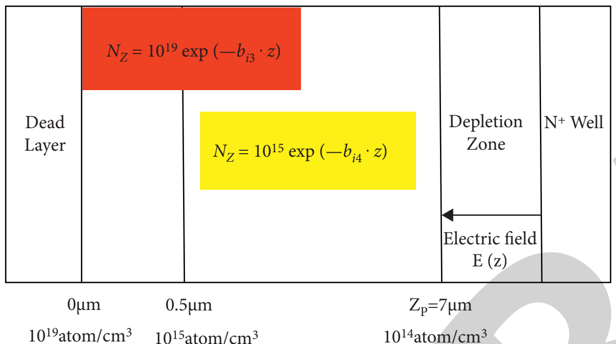

Figure 9: Electron multiplication layer multisegment exponential doping structure model 2.

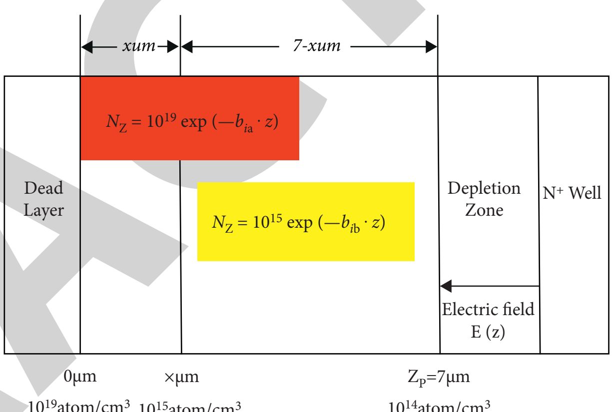

Figure 11: Model of multisegment exponential doping structure of electron multiplication layer.

The electron distribution in the 5 × 5 region at this time is shown in Figure 10, and the final charge collection efficiency obtained is 86.35%.

It can be seen that a thin exponential heavily doped layer near the dead layer side can effectively improve the charge collection efficiency. We further thinned the thickness of the exponentially heavily doped layer, and the model of the electron multiplication layer is shown in Figure 11, and the relationship between the thickness of the exponentially heavily doped layer and the charge collection efficiency is given in Table 1.

Analyzing these results, it is clear that the thinning of the exponentially heavily doped layer is beneficial to enhance the charge collection efficiency, and $N_Z = 10^{19}\exp(-b_{ia} \cdot z)$ for heavy exponential doping when $0 < z < 0.1$, $N_Z = 10^{15}\exp(-b_{ib} \cdot z)$ for light exponential doping when $0.1 < z < 7$, and $N_{0.1} = 10^{15}$atom/cm^3, at which the maximum charge collection efficiency of 94.48% is obtained. At this point, if the thickness of the exponentially heavily doped layer is further reduced, the charge collection efficiency starts to gradually decrease, which we speculate because an excessively thick exponentially lightly doped layer makes the strength of the gradient electric field in the exponentially lightly doped layer decrease, along with the increase in the thickness of the exponentially lightly doped layer, which makes the drift rate of the nonequilibrium carriers decrease and increases the compound rate of the electron-hole pairs, which eventually makes the charge collection efficiency affected.

Table 1: Effect of the thickness of the heavy index doping layer on the charge collection efficiency.

Thickness	0.3	0.2	0.1	0.05	0.03	0.01
CCE	89.42%	91.88%	94.48%	93.11%	90.14%	81.66%

5. Conclusion

Based on semiconductor theory, a computational model was developed to determine the effect of different doping methods on the charge collection efficiency in EBCMOS. When the *P*-type silicon substrate is uniformly doped, an electric field exists only in the depletion region, and no electric field can be generated at the electron multiplication layer. Exponential doping of *P*-type silicon substrates can produce a gradient electric field that facilitates the transport of multiplying electrons. If the *P*-type silicon substrate is exponentially doped as a whole, the high impurity concentration in the electron multiplication layer reduces the minority carriers' lifetime and the obtained charge collection

RETRACTED

efficiency is low. To solve this problem, we designed a multistage exponential doping structure of the electron multiplication layer. The thinner heavy exponential doping layer reduces the compounding probability of multiplying electrons in this region, while the suitable doping structure ensures the strength of the built-in electric field and the diffusion of multiplying electrons. Set the incident electron energy to 4 keV, the electron beam diameter to 20 nm, the dead layer thickness to 60 nm, and the thickness of the *P*-type silicon epitaxial layer to 10 μm. The simulation results show that the thinner exponential heavily doped layer can obtain the ideal charge collection efficiency in the range of $0 < z < 0.1\,\mu$m with $N_Z = 10^{19}\exp(-b_{ia}\cdot z)$, and in the range of $0.1 < z < 7\,\mu$m with $N_Z = 10^{15}\exp(-b_{ib}\cdot z)$ for exponential doping with $N_{0.1} = 10^{15}$atom/cm^3, when the maximum charge collection efficiency of 94.48% was obtained.

Data Availability

The dataset can be accessed upon request.

Conflicts of Interest

The authors declare that they have no conflicts of interest.

References

[1] T. Cajgfinger, A. Dominjon, and R. Barbier, "Single photon detection and localization accuracy with an ebCMOS camera," *Nuclear Instruments and Methods in Physics Research Section A: Accelerators, Spectrometers, Detectors and Associated Equipment*, vol. 787, pp. 176–181, 2015.

[2] L. Qi, F. Just, G. Leuchs, and M. V. Chekhova, "Autonomous absolute calibration of an ICCD camera in single-photon detection regime," *Optics Express*, vol. 24, no. 23, pp. 26444–26453, 2016.

[3] A. Shymanska, "Numerical analysis of electron optical system with microchannel plate," *Journal of Computational Electronics*, vol. 10, no. 3, pp. 291–299, 2011.

[4] M. S. Robbins and B. J. Hadwen, "The noise performance of electron multiplying charge-coupled devices," *IEEE Transactions on Electron Devices*, vol. 50, no. 5, pp. 1227–1232, 2003.

[5] C. D. Mackay, R. N. Tubbs, R. Bell, and D. J. Burt, "Sub-electron read noise at MHz pixel rates," *IS&T/SPIE Electronic Imaging*, vol. 4306, pp. 289–298, 2001.

[6] T. Brugière, F. Mayer, P. Fereyre, C. Guerin, A. Dominjon, and R. Barbier, "First measurement of the in-pixel electron multiplying with a standard imaging CMOS technology: study of the EMCMOS concept," *Nuclear Instruments and Methods in Physics Research Section A: Accelerators, Spectrometers, Detectors and Associated Equipment*, vol. 787, pp. 336–339, 2015.

[7] G. A. Vree, A. Westra, I. Moody, F. van der Have, K. Ligtvoet, and F. Beekman, "Photon-counting gamma camera based on an electron-multiplying CCD," *IEEE Transactions on Nuclear Science*, vol. 52, no. 3, pp. 580–588, 2005.

[8] R. Barbier, J. Baudot, E. Chabanat et al., "Performance study of a MegaPixel single photon position sensitive photodetector EBCMOS," *Nuclear Instruments and Methods in Physics Research Section A: Accelerators, Spectrometers, Detectors and Associated Equipment*, vol. 610, no. 1, pp. 54–56, 2009.

[9] L. M. Hirvonen and K. Suhling, "Photon counting imaging with an electron-bombarded pixel image sensor," *Sensors*, vol. 16, no. 5, p. 617, 2016.

[10] J. A. Levitt, P. Chung, M. K. Kuimova et al., "Fluorescence anisotropy of molecular rotors," *ChemPhysChem*, vol. 12, no. 3, pp. 662–672, 2011.

[11] S. B. Sobottka, T. Meyer, M. Kirsch et al., "Evaluation of the clinical practicability of intraoperative optical imaging comparing three different camera setups," *Biomedical engineering*, vol. 58, no. 3, pp. 237–248, 2013.

[12] M. Rossi, F. Casali, S. Golovkin, and V. Govorun, "Digital radiography using an EBCCD-based imaging device," *Applied Radiation and Isotopes*, vol. 53, no. 4-5, pp. 699–709, 2000.

[13] L. Benussi, V. Fanti, D. Frekers et al., "A multichannel single-photon sensitive detector for high-energy physics: the megapixel EBCCD," *Nuclear Instruments and Methods in Physics Research Section A: Accelerators, Spectrometers, Detectors and Associated Equipment*, vol. 442, no. 1-3, pp. 154–158, 2000.

[14] A. Suzuki, S. Aoki, J. Haba, M. Sakuda, and M. Suyama, "Novel large aperture EBCCD," *Nuclear Instruments and Methods in Physics Research Section A: Accelerators, Spectrometers, Detectors and Associated Equipment*, vol. 628, no. 1, pp. 260–263, 2011.

[15] V. W. Aebi and J. J. Boyle, "Electron Bombarded Active Pixel sensor," United States, 2001.

[16] https://www.intevac.com/intevacphotonics/ebaps-technology-overview.

[17] "I. NightVista VISNIR Low Light Cameras [EB/OL]," 2015, https://www.intevac.com/intevac-photonics/nightvista/.

[18] R. Barbier, P. Depasse, J. Baudot, and W. Dulinski, "First results from the development of a new generation of hybrid photon detector: EBCMOS," *Astroparticle, Particle And Space Physics, Detectors And Medical Physics Applications*, vol. 1, pp. 23–27, 2008.

[19] R. Barbier, T. Cajgfinger, P. Calabria et al., "A single-photon sensitive ebCMOS camera: the LUSIPHER prototype," *Nuclear Instruments and Methods in Physics Research Section A: Accelerators, Spectrometers, Detectors and Associated Equipment*, vol. 648, no. 1, pp. 266–274, 2011.

[20] A. Dominjon, M. Ageron, R. Barbier et al., "An ebCMOS camera system for marine bioluminescence observation: the LuSEApher prototype," *Nuclear Instruments and Methods in Physics Research Section A: Accelerators, Spectrometers, Detectors and Associated Equipment*, vol. 695, pp. 172–178, 2012.

[21] D. Fernández, J. Ricart, and J. Madrenas, "Experiments on the release of CMOS-micromachined metal layers," *Journal of Sensors*, vol. 2010, p. 7, 2010.

[22] C. G. Coates, D. J. Denvir, N. G. McHale, K. D. Thornbury, and M. A. Hollywood, "Optimizing low-light microscopy with back-illuminated electron multiplying charge-coupled device: enhanced sensitivity, speed, and resolution," *Journal of Biomedical Optics*, vol. 9, no. 6, pp. 1244–1252, 2004.

[23] R. Shimizu, Y. Kataoka, T. Ikuta, T. Koshikawa, and H. Hashimoto, "A Monte Carlo approach to the direct simulation of electron penetration in solids," *Journal of Physics D: Applied Physics*, vol. 9, no. 1, pp. 101–113, 1976.

[24] G. Buică, "Polarization dependence in inelastic scattering of electrons by hydrogen atoms in a circularly polarized laser field," *Journal of Quantitative Spectroscopy and Radiative Transfer*, vol. 187, pp. 190–203, 2017.

[25] X. Zhang, W. Fan, J. Xi, and L. He, "14-Bit fully differential SAR ADC with PGA used in readout circuit of CMOS image sensor," *Journal of Sensors*, vol. 2021, Article ID 6651642, 17 pages, 2021.

RETRACTED

[26] W. Dulinski, A. Braem, M. Caccia et al., "Tests of a backside illuminated monolithic CMOS pixel sensor in an HPD set-up," *Nuclear Instruments and Methods in Physics Research Section A: Accelerators, Spectrometers, Detectors and Associated Equipment*, vol. 546, no. 1-2, pp. 274–280, 2005.

[27] G. Deptuch, W. Dulinski, M. Caccia, and M. Winter, "High-resolution, back-side illuminated monolithic active pixel sensor for low-energy electron imaging," *IEEE Transactions on Nuclear Science*, vol. 52, no. 5, pp. 1745–1754, 2005.

[28] J. Hynecek, "Impactron-a new solid state image intensifier," *IEEE Transactions on Electron Devices*, vol. 48, no. 10, pp. 2238–2241, 2001.

[29] L. M. Hirvonen, M. J. Barber, and K. Suhling, "Photon counting imaging and centroiding with an electron-bombarded CCD using single molecule localisation software," *Nuclear Instruments and Methods in Physics Research Section A: Accelerators, Spectrometers, Detectors and Associated Equipment*, vol. 820, pp. 121–125, 2016.

[30] M. S. Alam, U. Manzoor, M. Mujahid, and A. S. Bhatti, "Highly responsive UV light sensors using Mg-doped ZnO nanoparticles," *Journal of Sensors*, pp. 1–5, 2016.

[31] L. M. Hirvonen, S. Jiggins, N. Sergent, G. Zanda, and K. Suhling, "Photon counting imaging with an electron-bombarded CCD: towards a parallel-processing photoelectronic time-to-amplitude converter," *Review of Scientific Instruments*, vol. 85, no. 12, Article ID 123102, 2014.

[32] J. Hynecek and T. Nishiwaki, "Excess noise and other important characteristics of low light level imaging using charge multiplying CCDs," *IEEE Transactions on Electron Devices*, vol. 50, no. 1, pp. 239–245, 2003.

[33] J. R. Fiebiger and R. S. Muller, "Pair-production energies in silicon and germanium bombarded with low-energy electrons," *Journal of Applied Physics*, vol. 43, no. 7, pp. 3202–3207, 1972.

[34] J. Bai, Y. Bai, X. Hou et al., "The analysis of electron scattering among multiplying layer in EBAPS using optimized Monte Carlo method," *Modern Physics Letters B*, vol. 34, no. 34, Article ID 2050398, 2020.

[35] A. Jablonski, "Multiple elastic scattering of electrons in condensed matter," *Computer Physics Communications*, vol. 210, pp. 92–102, 2017.

[36] R. Browning, T. Z. Li, B. Chui et al., "Empirical forms for the electron/atom elastic scattering cross sections from 0.1 to 30 keV," *Journal of Applied Physics*, vol. 76, no. 4, pp. 2016–2022, 1994.

[37] N. A. E. Nohy, N. E. Aly, A. M. Abdel-Moneim, and A. F. Hamza, "Dirac calculations for proton inelastic scattering at intermediate energies," *Brazilian Journal of Physics*, vol. 46, no. 6, pp. 714–720, 2016.

[38] Y. G. Xiao, K. Uehara, Y. Fu et al., "Toward designing back-illuminated CMOS image sensor based on 3D modeling," *Physics and Simulation of Optoelectronic Devices XXIV*, vol. 9742, pp. 30–37, 2016.

[39] C. M. Lee, S. P. Chang, S. J. Chang, and C. I. Wu, "p-Type quasi-mono silicon solar cell fabricated by ion implantation," *International Journal of Photoenergy*, vol. 2013, no. 1, Article ID 171390, 8 pages, 2013.

[40] A. Bentabet and N. Fenineche, "Backscattering coefficients for low energy positrons and electrons impinging on bulk solid targets," *Journal of Physics: Condensed Matter*, vol. 21, no. 9, Article ID 95403, 2009.

[41] L. M. Hirvonen, S. Jiggins, N. Sergent, G. Zanda, and K. Suhling, "Photon counting imaging with an electron-bombarded CCD: towards wide-field time-correlated single photon counting," *Nuclear Instruments and Methods in Physics Research Section A: Accelerators, Spectrometers, Detectors and Associated Equipment*, vol. 787, pp. 323–327, 2015.

[42] W. Wang, Y. Li, W. Chen, D. Song, and X. Wang, "Simulation of the electrostatic distribution in the proximity focusing structure of an EBCMOS," *IEEE Photonics Journal*, vol. 12, no. 3, pp. 1–10, 2020.

RETRACTED